

Article

# Direct Dimethyl Carbonates Synthesis over CeO<sub>2</sub> and Evaluation of Catalyst Morphology Role in Catalytic Performance

Ashif H. Tamboli<sup>1,2</sup>, Norihiro Suzuki<sup>3,4</sup> , Chiaki Terashima<sup>3,4,5</sup> , Suresh Gosavi<sup>1,3,\*</sup>, Hern Kim<sup>6,\*</sup> and Akira Fujishima<sup>3</sup>

- <sup>1</sup> Center for Advance Studies in Material Science and Solid State Physics, Department of Physics, Savitribai Phule Pune University (Formerly University of Pune), Pune 411007, India; tamboli90@gmail.com
- <sup>2</sup> Mass Dye Chem. Pvt Ltd., MIDC Bhosari, Pune 411026, India
- <sup>3</sup> Photocatalysis International Research Center, Research Institute for Science and Technology, Tokyo University of Science, 2641 Yamazaki, Noda, Chiba 278-8510, Japan; suzuki.norihiro@rs.tus.ac.jp (N.S.); terashima@rs.tus.ac.jp (C.T.); fujishima\_akira@admin.tus.ac.jp (A.F.)
- <sup>4</sup> Research Center for Space Colony, Tokyo University of Science, 2641 Yamazaki, Noda, Chiba 278-8510, Japan
- <sup>5</sup> Research Initiative for Supra-Materials, Shinshu University, Nagano 380-8553, Japan
- <sup>6</sup> Department of Energy Science and Technology, Environment Waste Recycle Institute, Myongji University, Yongin 17058, Gyeonggi-do, Korea
- \* Correspondence: swg@physics.unipune.ac.in (S.G.); hernkim@mju.ac.kr (H.K.)

**Abstract:** In recent years, direct synthesis of dimethyl carbonate (DMC) from carbon dioxide (CO<sub>2</sub>) has received considerable attention due to green and sustainable technology. Here, we report a production of DMC from major greenhouse gases and CO<sub>2</sub> using various morphologies of cerium oxide (CeO<sub>2</sub>). Time-dependent synthesis of CeO<sub>2</sub>, with controlled morphology having various shapes including sphere, nanorods and spindle shape, along with its formation mechanism is proposed. The experimental results indicate the morphology of CeO<sub>2</sub> was mostly dependent on the reaction time where crystal growth occurred through Ostwald ripening. The morphology, size and shape of CeO<sub>2</sub> were observed using transmission electron microscopy (TEM) and field emission scanning electron microscopy (FESEM). The crystallographic analysis using X-ray diffraction (XRD) shows cubic fluorite phase of CeO<sub>2</sub> with crystallite size ~72.0 nm using the Debye–Scherrer equation. The nitrogen adsorption desorption technique suggested the formation of the highly mesoporous framework of CeO<sub>2</sub> and the excellent surface area around 104.5 m<sup>2</sup>/g obtained for CeO<sub>2</sub> spindles by Brunauer–Emmett–Teller (BET) method. The DMC synthesis reactions were studied over CeO<sub>2</sub> catalyst with different morphologies. The results of catalytic reactions specify that the morphology of catalyst plays an important role in their catalytic performances, where spindle shape CeO<sub>2</sub> was the most active catalyst producing of up to 13.04 mmol of DMC. Furthermore, various dehydrating agents were used to improve the DMC production at optimized reaction parameters. The overall results reveal that the higher surface area and spindle shape of CeO<sub>2</sub> makes it a useful, reusable catalyst for one-pot DMC synthesis.

**Keywords:** carbon dioxide; cerium oxide; material morphology; dimethyl carbonate



**Citation:** Tamboli, A.H.; Suzuki, N.; Terashima, C.; Gosavi, S.; Kim, H.; Fujishima, A. Direct Dimethyl Carbonates Synthesis over CeO<sub>2</sub> and Evaluation of Catalyst Morphology Role in Catalytic Performance. *Catalysts* **2021**, *11*, 223. <https://doi.org/10.3390/catal11020223>

Academic Editor: Maria J. Sabater  
Received: 15 December 2020  
Accepted: 28 January 2021  
Published: 8 February 2021

**Publisher's Note:** MDPI stays neutral with regard to jurisdictional claims in published maps and institutional affiliations.



**Copyright:** © 2021 by the authors. Licensee MDPI, Basel, Switzerland. This article is an open access article distributed under the terms and conditions of the Creative Commons Attribution (CC BY) license (<https://creativecommons.org/licenses/by/4.0/>).

## 1. Introduction

Single-step synthesis of dimethyl carbonate (DMC) has paid considerable attention to the research community in past two decades because of the utilization of CO<sub>2</sub>, which is a chief offender of the greenhouse effect [1–3]. Although various routes have been reported for the conversion of CO<sub>2</sub> to valuable chemicals, DMC was found to be a priority due to its remarkable properties and numerous applications [4,5]. The important feature of DMC is its utilization of CO<sub>2</sub> as a building block for useful organic chemicals by replacing conventional fossil fuels. Additionally, DMC has been widely used as additive in fuel, due

to its good blending properties, higher oxygen content and most importantly, it shows a favorable water/fuel partition coefficient along with an insignificant effect on environment. Furthermore, it was explored for its application and use in pharmaceuticals, polycarbonate, agrochemicals, antioxidants, adhesives, electrolytes, and as budding solvents in lithium ion batteries [5–8]. Although direct DMC synthesis was considered a green and sustainable route, it suffers from thermodynamic and kinetic limitations [9]. Therefore, the designing of novel catalyst materials and efficiently taking water away from the reaction system are the challenges for researchers.

In general, metal oxides possess both redox and acid/base properties, which are essential for absorption and catalysis reactions [10,11]. Interestingly the literature reveals that especially CeO<sub>2</sub> and zirconium oxide (ZrO<sub>2</sub>) are highly active catalysts for direct DMC synthesis from CO<sub>2</sub> and methanol [12–15]. Several studies have reported on CeO<sub>2</sub>/ZrO<sub>2</sub> catalysts for kinetics and elaborated equilibrium model [16,17]. Recently, a group of researchers achieved the highest results (i.e., >95% methanol conversion and >99% of DMC selectivity) for CeO<sub>2</sub> catalyst in combination with 2-cyanopyridine dehydrating agent in a continuous system [18]. Based on the literature review, it can be concluded that CeO<sub>2</sub> is a best heterogeneous catalyst for direct DMC synthesis and their catalytic activity is mostly dependent on the structural, morphological and acidic/basic properties [19]. Additionally, CeO<sub>2</sub> has gained tremendous interest for its wide range of applications in recent days owing to their excellent acid/base properties and oxygen storage capacities. However, the morphology and DMC formation mechanism over CeO<sub>2</sub> must be addressed to achieve modified catalyst properties and improved its catalytic performance [20].

At the nanoscale, CeO<sub>2</sub> catalysts are much more efficient as a result of their improved surface areas and/or surface properties, formation of oxygen vacancies in high number and better oxygen storage ability [21]. The enhanced catalytic activity can be achieved even at low temperatures and can be further boosted by tailoring novel morphology at the nanoscale level, attributing to exposure of highly reactive crystal planes such as 111, 100 and 110 to achieve improved catalytic activity [22]. Therefore, the finding of suitable synthesis approach for the morphological control over nanometer size CeO<sub>2</sub>, that can act as an active catalyst even at a lower temperature is still a major landmark. Interestingly some researchers have reported that the morphologies of CeO<sub>2</sub> directly affect the catalytic activity for DMC synthesis. A collective synergistic effect of defect sites, acid-base sites and exposed 111 plane are crucial for achieving high DMC conversion [23,24]. Spindle-shaped CeO<sub>2</sub> shows highest DMC production than nanorods, nanocubes and nano-octahedrons.

Despite several reports available in the literature on direct DMC synthesis over CeO<sub>2</sub>, the activity, morphology, surface area and reaction mechanism are still challenging aspects for the researchers and must be addressed. Inspired by the above facts, we take this opportunity to synthesize CeO<sub>2</sub> catalysts with novel morphology and excellent surface area, and acid/base and redox properties using a simple and cost-effective synthesis method [25]. Therefore, in this work, we propose a stepwise DMC formation mechanism, which would be a great achievement in the catalytic development.

The objectives of this study are: (i) To synthesize a highly efficient CeO<sub>2</sub> catalyst with a different morphology using a cost-effective method; (ii) Investigate the formation mechanism of CeO<sub>2</sub> using a time-dependent material synthesis experiments; (iii) Use of synthesized CeO<sub>2</sub> materials as catalysts for conversion of CO<sub>2</sub> and methanol into DMC; and (iv) Evaluate the effect of catalyst morphology on the catalytic performance and role of dehydrating agents. An attempt was also made to investigate the reaction mechanism using experimental results and Fourier-transform infrared spectroscopy (FTIR) studies of the catalyst material before and after the reaction.

## 2. Results and Discussion

### 2.1. Characterization of CeO<sub>2</sub>

The CeO<sub>2</sub> formation mechanism is proposed with the help of microscopic results, where the samples (with time intervals 8, 10, 12 and 16 h) were analyzed using SEM. These experiments suggest that synthesis time is very important in the evolution of morphologies of CeO<sub>2</sub> in ambient conditions. Figure 1A–H shows SEM analysis results of the calcined CeO<sub>2</sub> nanostructure. As can be seen, minor CeO<sub>2</sub> particles are formed first, which further develop to become a bigger particles due to Ostwald ripening. This means the solid solutions formed into the reaction medium, which described the growth mechanism of inhomogeneous or dissimilar structure over time. The process begins by phase precipitation of CeO<sub>2</sub> solid with a well-defined spherical shape; the energetic factors will move towards forming better precipitates to develop through attaching minor CeO<sub>2</sub> precipitates (sphere) on the bigger particle surface [26]. Thermodynamic factors could also be accountable for the amount of this effect where smaller CeO<sub>2</sub> sphere are stable than bigger particles (sphere with bigger particles) and reverse relative internal pressure to radius of the particle [27]. The main factor for the above cause could be the occurrence of less stable particles on CeO<sub>2</sub> particles surface than finely arranged in the framework (Figure 1A,B).

The lower surface energy of large CeO<sub>2</sub> particles (mixed shapes) is due to the lower surface to volume ratio of precipitation. The particles from the surface of energetically unstable small CeO<sub>2</sub> sphere evade and diffuse through the solution and get attached to the surface of larger particles during the lowering of overall energy of a system [28]. Smaller CeO<sub>2</sub> sphere goes on disappearing with the synchronized progress in the growth of bigger CeO<sub>2</sub> particles. This mechanism can be explained by the fact that the highest probability of molecules concentration in the environs of smaller CeO<sub>2</sub> sphere than the average number in total solution. These tiny CeO<sub>2</sub> spheres along with bigger particles move towards less concentrated from more concentrated solution phase by diminishing total amount of tiny sphere particles. In contrast, lower concentration in the closeness of bigger CeO<sub>2</sub> particles than normal concentration in entire solution enable diffusion of particles to the bigger CeO<sub>2</sub> particles from solution phase (Figure 1C,D). Hence, both the particle size and concentration gradient around the particle are responsible for rate of Ostwald ripening. Interestingly further increase in reaction time resulted into distinct spindle-like morphology of CeO<sub>2</sub> nanostructure (Figure 1E,F). Nevertheless, high reaction time leads to the formation of long rods by merging of CeO<sub>2</sub> spindles (Figure 1G,H). The results suggest that well-defined CeO<sub>2</sub> spindle morphology can be achieved by 12 h synthesis time and annealing CeO<sub>2</sub> at 500 °C.

The possible growth mechanism of CeO<sub>2</sub> is proposed even though the real formation mechanism is still uncertain. The precipitation process involves a number of chemical reactions using urea as precipitating agent. Process begins with the hydrolysis of urea by formation of NH<sub>4</sub><sup>+</sup> and OH<sup>−</sup> ions. The OH<sup>−</sup> ion then reacts with Ce ion to get Ce(OH)<sub>3</sub> solid precipitate. The basic pH can be achieved by the existence of NH<sub>4</sub><sup>+</sup> ions in the reaction medium, which is required for the precipitation process. Finally, the obtained precipitate was separated by simple filtration with thorough distilled water and ethanol washing and annealed at high temperatures to manage various CeO<sub>2</sub> morphologies such as sphere, spindle and nanorods. In the whole precipitation process, urea concentration and reaction temperature apparently come into play [29–31].

The morphology studies of CeO<sub>2</sub> samples investigated using TEM and HRTEM analysis techniques. Figure 2A–L displays the characteristic TEM, HRTEM and SAED images of the CeO<sub>2</sub> morphologies i.e., sphere, mixed shape, spindle and nanorods. These observations are well in agreement with SEM analysis results. The morphology of CeO<sub>2</sub> spindle composed of several small particles attached in a row.

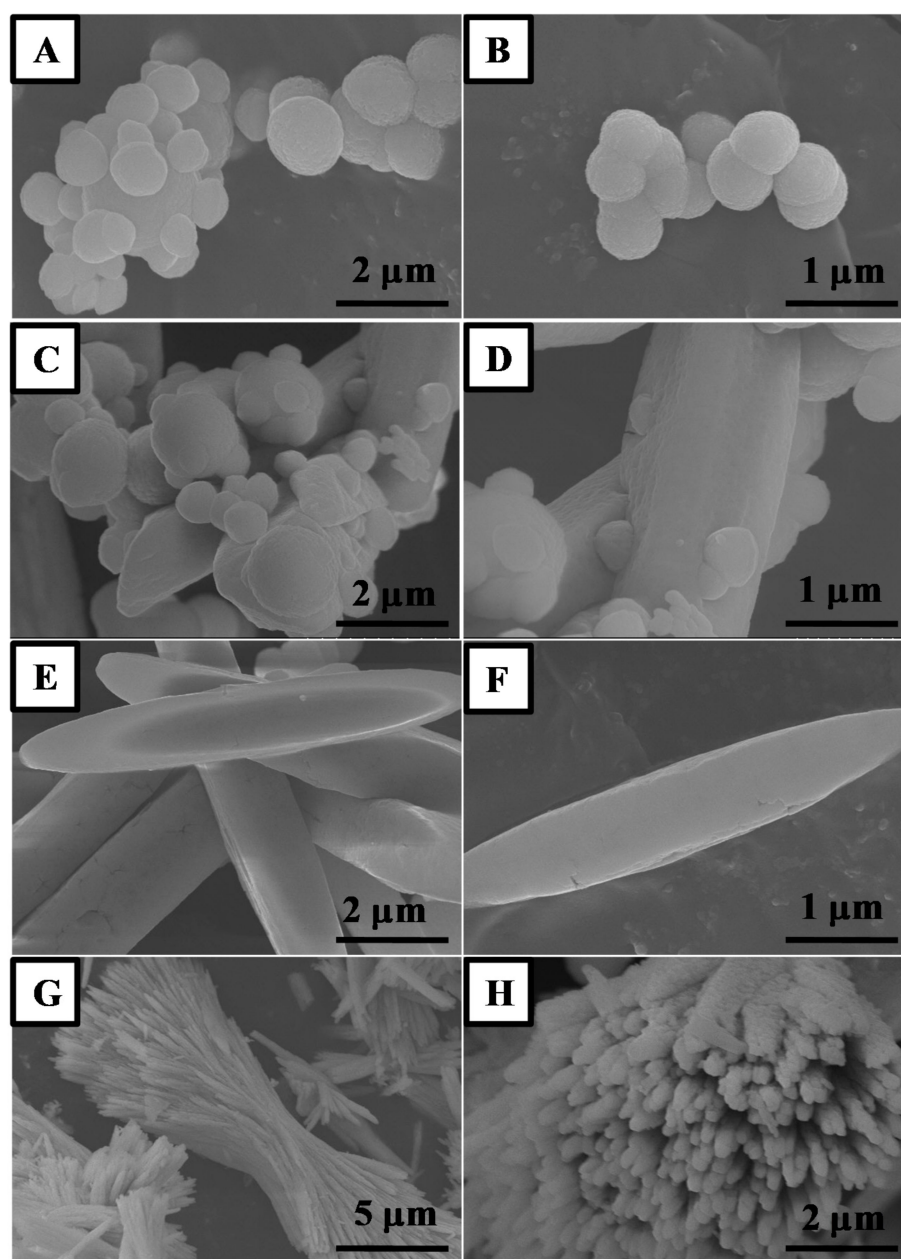


**Figure 1.** Low to high magnification Field-emission Scanning Electron Microscope (FESEM) images of the CeO<sub>2</sub> sphere (A,B); mixed shape CeO<sub>2</sub> (C,D); CeO<sub>2</sub> spindles (E,F) and CeO<sub>2</sub> nanorods (G,H) prepared by annealing Ce(OH)<sub>3</sub> at 500 °C for 3 h.

The average diameter of CeO<sub>2</sub> spindles is roughly 103 nm and  $1467 \pm 91$  nm in length suggesting shrinking of spindles by decreasing its size after calcinations. The SAED patterns of Spheres (8h-CeO<sub>2</sub>), mixed shape (10h-CeO<sub>2</sub>), spindles (12h-CeO<sub>2</sub>) and nanorods (12h-CeO<sub>2</sub>) are in agreement with XRD results. Furthermore, HRTEM images of prepared CeO<sub>2</sub> samples reveals dotted lines and rod axis are parallel to each other. The dotted line spacing is 3.11 Å that is concurred accurately with the (111) plane.

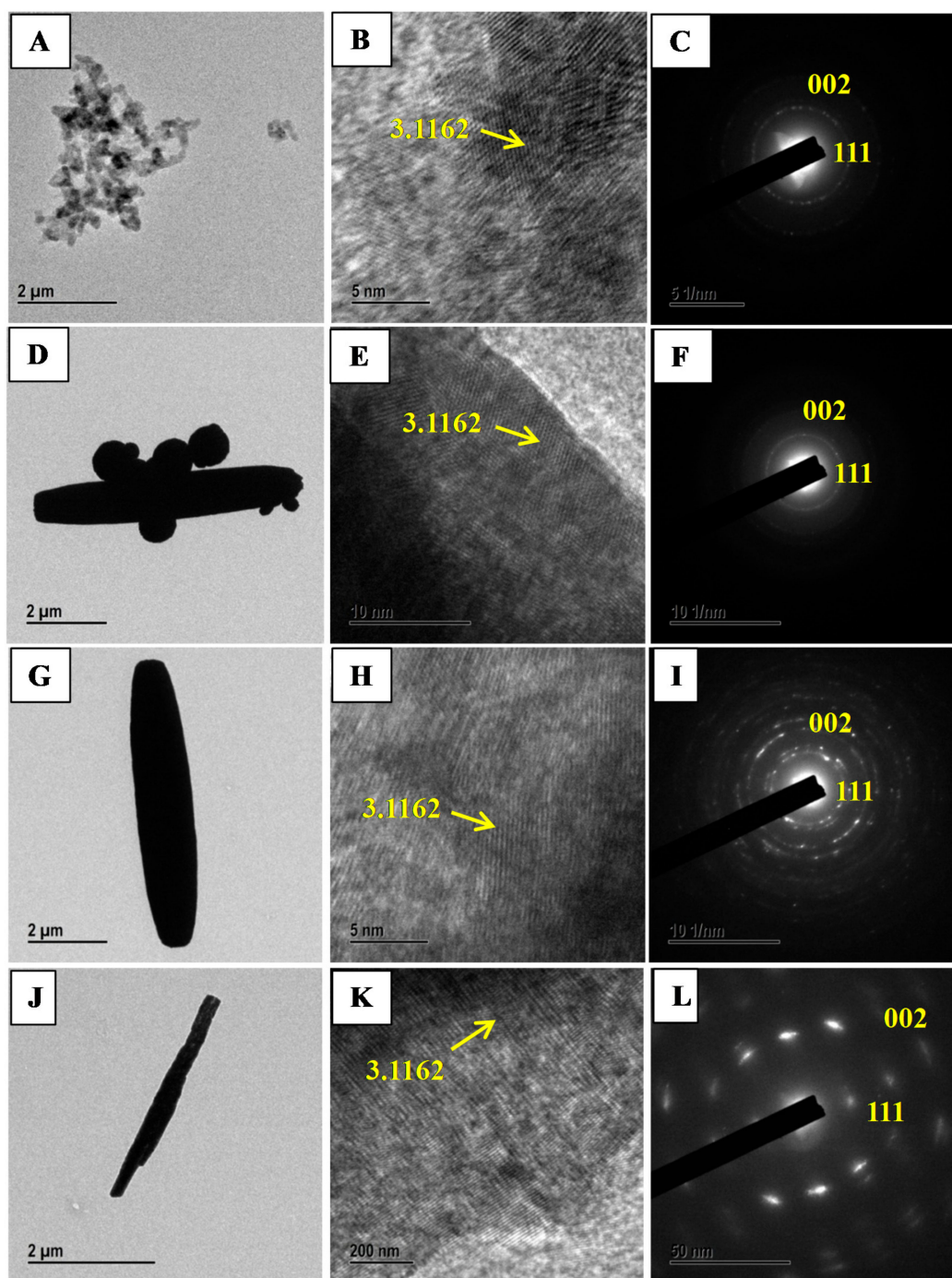


**Figure 2.** Transmission electron microscopy (TEM), High-resolution transmission electron microscopy (HRTEM), and selected area electron diffraction (SAED) images of SphereCeO<sub>2</sub> (A–C); mixed shape CeO<sub>2</sub> (D–F); CeO<sub>2</sub> spindles (G–I) and CeO<sub>2</sub> nanorods (J–L) prepared by annealing Ce(OH)<sub>3</sub> at 500 °C for 3 h.

Metal oxides are invaluable and tunable materials with improved morphology surface area or porosity at molecular level having wide range of applications in organic synthesis, catalysis, electrochemistry, etc., fields. The structural properties of CeO<sub>2</sub> were investigated by the nitrogen adsorption/desorption method. In Figure 3A, H<sub>2</sub> hysteresis loop of relative pressure range through  $0.50 < P/P_0 < 0.97$  suggest presence of type IV isotherm for sphere-shaped CeO<sub>2</sub> prepared at 8 h reaction time.

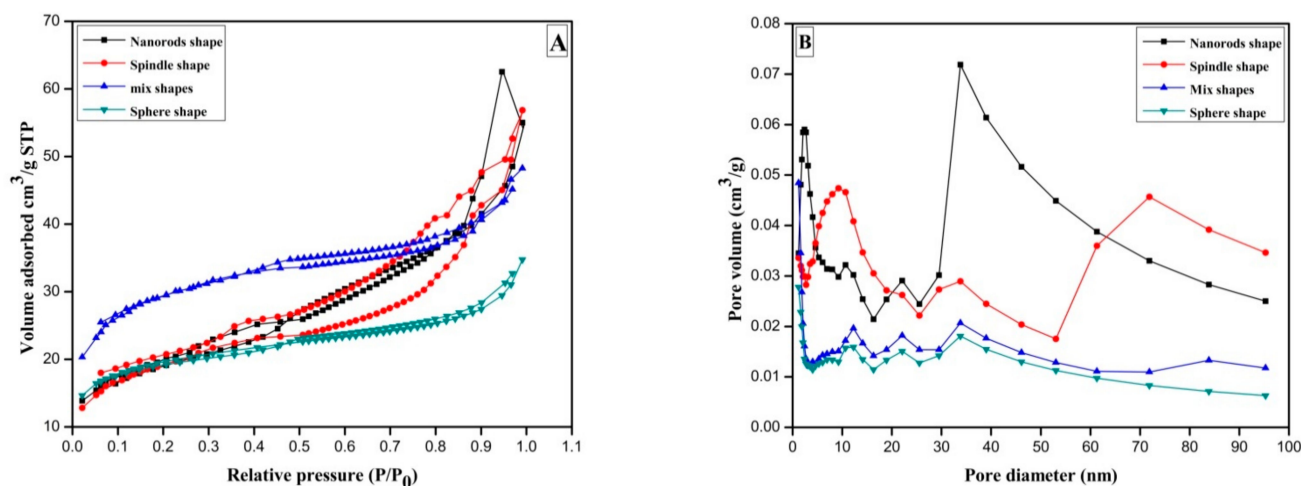


**Figure 3.** (A) N<sub>2</sub> adsorption-desorption curve of the CeO<sub>2</sub> sphere; mixed shape CeO<sub>2</sub>; CeO<sub>2</sub> spindle and CeO<sub>2</sub> nanorods prepared by annealing Ce(OH)<sub>3</sub> at 500 °C for 3 h; (B) Barrett-Joyner-Halenda (BJH) plots of CeO<sub>2</sub> samples.

For the mixed shape morphology of CeO<sub>2</sub> synthesized for 10 h, the hysteresis circle of type IV-type isotherm was witnessed with a relative pressure of  $0.44 < P/P_0 < 0.96$ . Furthermore, spindle-shaped CeO<sub>2</sub> displays a typical type IV isotherm following H<sub>2</sub> type hysteresis curve in relative pressure range of  $0.30 < P/P_0 < 0.97$ . Usually they are cage-like pore structures and numerous mesopores accompanied by narrow channel linkages. On the other hand, nanorods synthesized in 16 h gives H<sub>2</sub> type hysteresis loop in relative pressure range of  $0.48 < P/P_0 < 0.83$ . The gases get condensed in minor capillary pores of sample at pressure lower than the saturation pressure of gas, i.e., formation of monolayer followed by multilayer in type-IV isotherm [32].

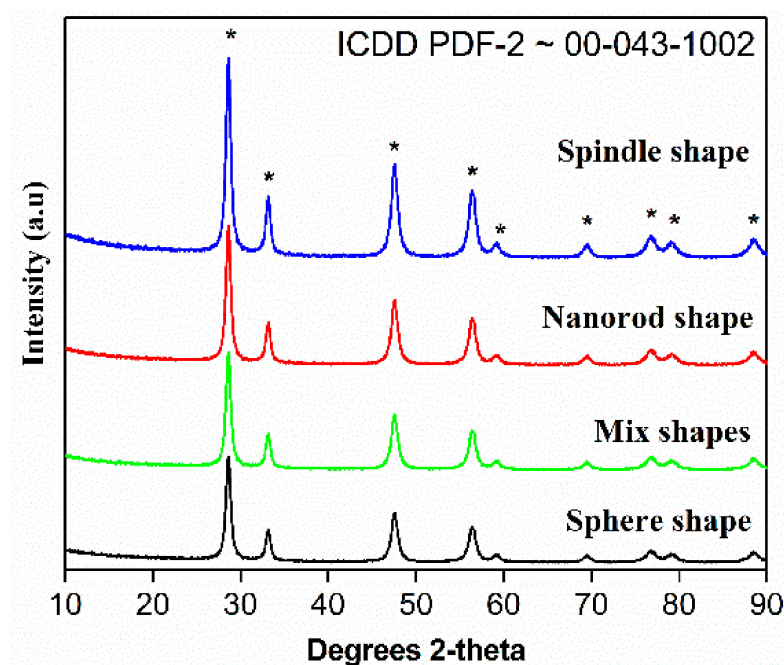
Moreover, pore size distribution analysis of CeO<sub>2</sub> was performed by nonlocal density functional theory (NLDFT) algorithm method. As shown in Figure 3B, micropores pointed at 1.19 nm and three mesopores distribution by 12.12, 22.11 and 33.85 nm can be seen for sphere shaped samples. Whereas, mixed shapes possessing sphere and spindle-shaped sample illustrated number of mesopores at 2.26, 10.52, 21.99 and a large peak just about 33.86 nm. The spindle-shaped CeO<sub>2</sub> sample exhibits single mesopores centered at 1.19 nm and many mesopores near 12.26, 21.90, 33.85 nm, correspondingly. That means sphere and spindle-shape CeO<sub>2</sub> samples consist of doubly hierarchical porous mesopores and micropores framework. Besides, the CeO<sub>2</sub> nanorods exhibited single micropores signal close to 1.19 nm whereas two 9.19 and 33.85 nm mesopores and a broad macropores centers at 71.92. The outcomes point out that the CeO<sub>2</sub> nano rods own triply hierarchical micropores, mesopores, and macropores framework. Additionally, the Brunauer–Emmett–Teller (BET) surface areas of Sphere CeO<sub>2</sub>, mixed shape CeO<sub>2</sub>, spindle CeO<sub>2</sub> and nanorod CeO<sub>2</sub> samples are 71, 66.8, 104.5 and 66.4 m<sup>2</sup>/g, respectively (Table 1; entries 1–4). The conclusion has been drawn from BET analysis results that increase of synthesis time starting at 8 h to 10 h considerably boosts surface area whereas additional increase of synthesis time to 12 h causes negative consequence on surface areas. In other words, spindle-shape CeO<sub>2</sub> exhibited highest surface area compared to other morphologies. As stated previously, initially formed sphere particles follow Ostwald ripening to grow until 12 h synthesis time resulting into highly mesopores mixed structures of CeO<sub>2</sub> spindles. Subsequent increase in synthesis time on the other hand leads to the development of long nanorods connecting nanoparticles to each other by decreasing surface to volume ratio. Furthermore, when synthesis time increased from 8 h to 12 h total pore diameter decreased from 3.0193 to 2.8157 nm which later reached at 5.1280, while further increase in synthesis time of up to 16 h (Table 1; entries 1–4). The hydroxyl groups of initially formed precipitate decompose into various CeO<sub>2</sub> structures (sphere, spindle, nanorods, etc.) after heat treatment at 500 °C.

**Table 1.** Brunauer–Emmett–Teller surface area CeO<sub>2</sub> samples and characteristic FTIR bands of DMC formation on the surface of CeO<sub>2</sub>.

Sr. No.	Catalyst	Surface Area (m <sup>2</sup> g <sup>-1</sup> )	Pore Volume (cm <sup>3</sup> g <sup>-1</sup> )	Pore Size (nm)
1	CeO <sub>2</sub> sphere	71	0.053	3.0
2	CeO <sub>2</sub> mixed shapes	68	0.094	5.4
3	CeO <sub>2</sub> spindles	104	0.073	2.8
4	CeO <sub>2</sub> nanorods	66	0.085	5.1

All surface values obtained from N<sub>2</sub> adsorption-desorption study and BET analysis.

The XRD patterns of CeO<sub>2</sub> calcined at 500 °C is presented in Figure 4. The cubic phase of CeO<sub>2</sub> was confirmed by the occurrence of most intense peak in the diffraction patterns. In brief,  $2\theta = 28.6, 33.1, 47.6$  and  $56.4$  diffraction peaks are assigned to (111), (200), (220) and (311), etc., planes of CeO<sub>2</sub> cubic fluorite phases.

**Figure 4.** XRD patterns of the CeO<sub>2</sub> sphere; mixed shape CeO<sub>2</sub>; CeO<sub>2</sub> spindle and CeO<sub>2</sub> nanorods prepared by annealing Ce(OH)<sub>3</sub> at 500 °C for 3 h.

These peaks grew in its intensity as the crystallization. These results obey ICDD PDF-2 ~00-043-1002 standard data along with the earlier studies. The absence of additional diffraction pattern suggests high purity of as-prepared CeO<sub>2</sub> and the phases confirm the formation of cubic fluorite phase of CeO<sub>2</sub> structures. It is important to note that 12 h-CeO<sub>2</sub> (spindle shape) shows highly intense peaks. The values of full width at half maxima of intense peaks used to calculate crystallite size  $d_{\text{Scherrer}}$  with the help of Scherrer equation. The calculated crystal size of CeO<sub>2</sub> using 111 plane Scherrer's equation calculated to be around 103 nm.

## 2.2. Catalytic Performance of CeO<sub>2</sub>

Catalytic activities of various CeO<sub>2</sub> catalysts are shown in Table 2. Only DMC was obtained as a product in the experiments. 12 h-CeO<sub>2</sub> catalyst (spindle shape) demonstrated the best catalytic activity (Table 2; entry 3), whose TOFh<sup>-1</sup> was almost double than that of the 8 h-CeO<sub>2</sub> (sphere shape) catalyst (Table 2; entry 1) and much higher than 10 h-CeO<sub>2</sub> (mix shape) and 16 h-CeO<sub>2</sub> (nanorod shape) (Table 2; entries 2 and 4), respectively. It indicates that the catalytic performances of all catalysts are mostly correlated

to the morphology and proportional to  $\text{CeO}_2$  synthesis time. The spindle-shape  $\text{CeO}_2$  catalysts exhibited higher  $\text{TOF h}^{-1}$  (0.748) than sphere (0.395) and  $\text{CeO}_2$  nanorods (0.588). On the other hand, the  $\text{CeO}_2$  catalyst with a mixed morphology of sphere and spindle produces  $0.566 \text{ TOF h}^{-1}$  in 3 h. These results are in agreement with the stated literature that the higher the acid/basic sites in catalysts higher will be the catalytic activity. Therefore, surface area, morphology and acidity/basicity of catalysts enhance the catalytic activity for DMC synthesis. The catalytic activity and morphologies have been compared in this work and the superior surface area to volume ratio, surface oxygen vacancies, and redox properties of  $\text{CeO}_2$  makes it even more attractive. These properties enable 111  $\text{CeO}_2$  crystal plane exposed to the interaction with reactants and enhance catalytic activity. Various studies supported this argument regarding the relation of 111 crystal plane of  $\text{CeO}_2$  and catalytic activity [14,23]. Hence, spindle-shaped  $\text{CeO}_2$  essentially have 111 crystal planes further open, resulting in the excellent catalytic activity for DMC production and these experimental results are supported by BET and XRD interpretations. As shown in Figure 5, spindle-type morphology produces highest  $\text{TOF h}^{-1}$  than nanorods followed by mixed structures of sphere plus spindles and then spherical nanoparticles. Besides, to optimize reaction conditions, DMC synthesis reactions have been carried out by varying parameters such as catalyst amount, temperature and pressure. The best catalyst found in the catalyst screening, i.e., spindle-shape  $\text{CeO}_2$  selected for the parametric study. The catalytic activity of spindle-shape  $\text{CeO}_2$  investigated to know the effect of pressure on the  $\text{TOF h}^{-1}$  by changing the pressure from 6.5 MPa to 8.0 MPa,  $140^\circ\text{C}$  temperature and 1 g catalyst amount (Table 2).

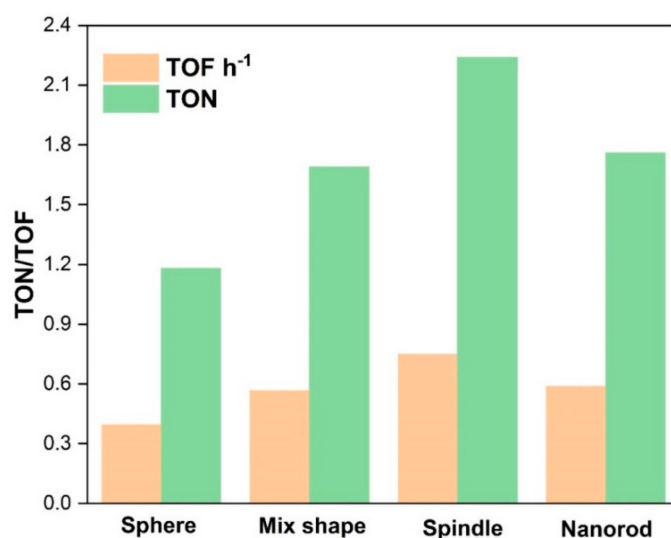


**Figure 5.** Catalytic activities of  $\text{CeO}_2$  catalysts for the synthesis of DMC with respective morphologies.

It was observed in these experiments that the pressure shows obvious role in DMC synthesis reaction where  $\text{TOF h}^{-1}$  continuously improved with the  $\text{CO}_2$  pressure. The results are in agreement with the previous studies in the literature regarding the relationship between catalyst activity and  $\text{CO}_2$  pressure. For 6.5 MPa pressure at  $140^\circ\text{C}$  after 3 h reaction  $0.507 \text{ TOF h}^{-1}$  was attained over spindle-shape  $\text{CeO}_2$  (Table 2; entry 5). Furthermore,  $0.589 \text{ TOF h}^{-1}$  obtained to 7 MPa pressure and  $140^\circ\text{C}$ , with the latter increasing at 7.5 MPa (See Table 2; entries 3 and 6). Spindle-shape  $\text{CeO}_2$  yields enhanced TOF, i.e.,  $0.794 \text{ h}^{-1}$  at the 8 MPa higher pressure (Table 2; entry 7). These results indicate that higher will be the DMC production at higher reaction pressure. Yet,  $\text{CO}_2$  manages an intermediate phase of gas and liquid at 7.39 MPa supercritical pressure of  $\text{CO}_2$  and it is obvious that liquid reactions are more reactive than gases. The catalyst activity enhanced when the pressure was increased 7 MPa to 7.5 MPa and the activity remains intact, although there is more of an increase. Therefore, the pressure near the  $\text{CO}_2$

supercritical pressure, i.e., 7.5 MPa seems good for direct conversion of CO<sub>2</sub> and methanol to DMC synthesis.

**Table 2.** Catalytic results for various catalysts and parameters used for DMC synthesis from CO<sub>2</sub> and methanol.

Sr. No.	<sup>b</sup> Catalyst	<sup>c</sup> Catalyst wt. (g)	<sup>a</sup> Dehydrating Agent	<sup>c</sup> Pressure (MPa)	<sup>c</sup> Temperature (°C)	<sup>d</sup> TON (M. s <sup>-1</sup> )	<sup>d</sup> TOF (h <sup>-1</sup> )
1	Sphere CeO <sub>2</sub>	1	-	7.5	140	1.18	0.395
2	Mixed shape CeO <sub>2</sub>	1	-	7.5	140	1.69	0.566
3	Spindle CeO <sub>2</sub>	1	-	7.5	140	2.24	0.748
4	Nanorod CeO <sub>2</sub>	1	-	7.5	140	1.76	0.588
5	Spindle CeO <sub>2</sub>	1	-	6.5	140	1.52	0.507
6	Spindle CeO <sub>2</sub>	1	-	7	140	1.76	0.589
7	Spindle CeO <sub>2</sub>	1	-	8	140	2.38	0.794
8	Spindle CeO <sub>2</sub>	1	-	7.5	100	1.65	0.553
9	Spindle CeO <sub>2</sub>	1	-	7.5	120	2.20	0.736
10	Spindle CeO <sub>2</sub>	1	-	7.5	160	2.25	0.751
11	Spindle CeO <sub>2</sub>	0.5	-	7.5	140	3.59	1.199
12	Spindle CeO <sub>2</sub>	1.5	-	7.5	140	1.68	0.561
13	Spindle CeO <sub>2</sub>	2	-	7.5	140	1.35	0.452
14	Spindle CeO <sub>2</sub>	1	Molecular sieve 4A	7.5	140	3.33	1.110
15	Spindle CeO <sub>2</sub>	1	DMP	7.5	140	4.31	1.439
16	Spindle CeO <sub>2</sub>	1	Acetonitrile	7.5	140	3.41	1.138
17	Spindle CeO <sub>2</sub>	1	Cyclohexene oxide	7.5	140	4.25	1.419
18	Spindle CeO <sub>2</sub>	1	Styrene oxide	7.5	140	4.29	1.433

<sup>a</sup> Reactions were carried out on 1 g of the dehydrating agent, and 618 mmol of methanol, <sup>b</sup> Catalyst, <sup>c</sup> Amount of catalyst, pressure, and temperature used for experiments, <sup>d</sup> TON M. s<sup>-1</sup> and TOF's h<sup>-1</sup> were determined by GC analysis. The products were analyzed by GC, GCMS, and FTIR.

The catalytic activity of spindle-shaped CeO<sub>2</sub> was assessed using constant amount (1 gm) of catalyst and 7.5 MPa CO<sub>2</sub> pressure, with variable reaction temperature ranging from 100 to 160 °C (See Table 2). As expected, the TOF h<sup>-1</sup> improved with increase in temperature with the exception of CeO<sub>2</sub> spindles. The TOF increased from 0.553 h<sup>-1</sup> to 0.736 h<sup>-1</sup> over CeO<sub>2</sub> spindle catalyst after 3 h when the temperature hiked from 100 to 120 °C, which later reaches to 0.748 h<sup>-1</sup> at 140 °C (Table 2; entries 8, 9 and 3). Conversely, no significant effect of 160 °C was witnessed on catalyst activity and remained at 0.751 h<sup>-1</sup> (See Table 2; entry 10). These results indicate that, reaction temperature only improves the TOF however the figures are not noteworthy. Overall, investigations suggested that, 140 °C is suitable and optimize temperature, for the conversion of CO<sub>2</sub> and methanol into DMC, using spindle-shape CeO<sub>2</sub>.

In order to investigate the effect of catalyst amount on the catalyst activity, systematic studies were carried out by varying amount of spindle-shape CeO<sub>2</sub> catalyst from 0.5 to 2 g at constant 140 °C temperature and 7.5 MPa pressure. Table 2 reveals that the TOFs decrease with an increase in catalyst amount. The 0.5 g spindle-shape CeO<sub>2</sub> catalyst turns out 1.119 TOFh<sup>-1</sup> following 3 h of reaction (Table 2; entry 11). As soon as the catalyst amount augmented to 1 g the TOF attained 0.748 h<sup>-1</sup> at 7.5 MPa pressure and 140 °C after 3 h of reaction (Table 2; entry 3). However, a value of more increase in catalyst quantity didn't have significant effect on catalyst activity and resulted into 0.561 h<sup>-1</sup> and 0.452 h<sup>-1</sup> of TOF for 1.5 and 2 g of catalyst, respectively (Table 2; entries 12 and 13). We can conclude from these experiments that even though there is a direct effect of the catalyst amount on the yield or catalytic performance by providing high number of catalysts active sites to the reaction, an excess catalyst amount is ineffective. Furthermore, these results were compared with the previously reported CeO<sub>2</sub> for the title reaction and it was found that our catalyst displayed excellent catalytic performance (Table 3).

In the development of catalyst systems for industrial applications, catalyst reusability studies are very important. Controlled experiments were performed for reusability of

spindle-shape CeO<sub>2</sub> catalyst, under best optimized reaction conditions i.e., 7.5 pressures, 140 °C, 1 g catalyst for five successive runs. After the completion of the reaction, the catalysts were recollected by simple filtration with thorough washing with distilled water followed by ethanol and then dried/stored for its reuse. It was observed from the reusability test results that the catalyst showed very good activity with a small decrease in the trend for subsequent runs (Figure 6). Typically, following the first run, the activity decreases minimally, remains almost constant after the fifth run, but the difference in catalytic activity is small. For this reason, spindle-shape CeO<sub>2</sub> would be potential catalyst for direct synthesis of DMC path with exceptional reusability.

**Table 3.** Comparative results of cerium oxide catalysts for the direct synthesis of DMC from CO<sub>2</sub> and methanol.

Catalysts	Dehydrating Agent	Temp. (°C)	Pressure (MPa)	DMC (mmol)	TOF (h <sup>-1</sup> )	References
CeO <sub>2</sub>	-	170	5	0.66	-	[33]
CeO <sub>2</sub>	CH <sub>3</sub> CN	150	0.5	1.52	-	[34]
Spindle-like CeO <sub>2</sub>	-	140	5	4.10	-	[35]
CeO <sub>2</sub>	-	140	5	5.34	-	[36]
CeO <sub>2</sub>	3 A MS	120	15	2.04	-	[37]
CeO <sub>2</sub> -4A	-	120	0.6	3.23	-	[38]
CeO <sub>2</sub> Spindle	-	140	8	13.84	0.794	[This study]
CeO <sub>2</sub> Spindle	Molecular sieve 4A	140	7.5	19.35	1.110	[This study]
CeO <sub>2</sub> Spindle	DMP	140	7.5	25.09	1.439	[This study]
CeO <sub>2</sub> Spindle	Acetonitrile	140	7.5	19.84	1.1380.	[This study]
CeO <sub>2</sub> Spindle	Cyclohexene oxide	140	7.5	24.75	1.419	[This study]
CeO <sub>2</sub> Spindle	Styrene oxide	140	7.5	24.98	1.433	[This study]
Molecular sieve 4A	-	140	7.5	0.09	-	[This study]

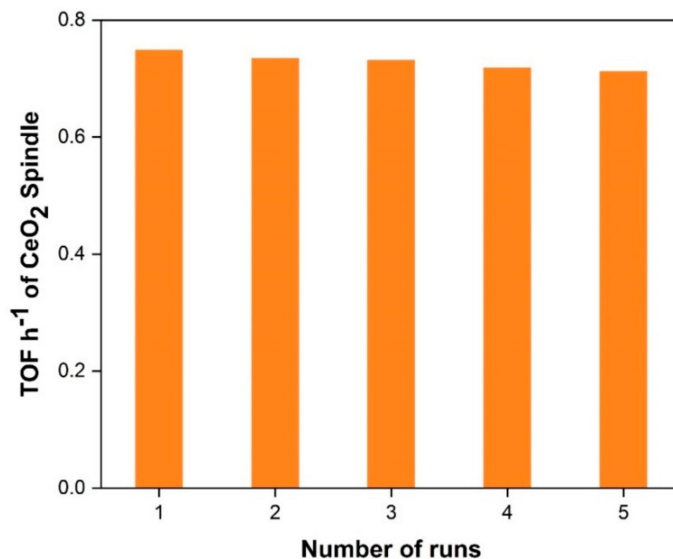


**Figure 6.** Reusability testing of spindle-shape CeO<sub>2</sub> for five consecutive runs.

In order to analyze CO<sub>2</sub> desorption properties on CeO<sub>2</sub>; 12 h-CeO<sub>2</sub> was used as a representative of CeO<sub>2</sub>-based CO<sub>2</sub> adsorbent assuming that other CeO<sub>2</sub> with similar surface condition would exhibit the similar desorption properties. Figure 7 shows CO<sub>2</sub> TPD curve of CeO<sub>2</sub> from 50 °C to 1050 °C. Each dot represents the amount of CO<sub>2</sub> desorbed during each 10 °C increment in temperature. For example, the dot at 50 °C represents the amount of CO<sub>2</sub> desorbed from 50 °C to 60 °C. CO<sub>2</sub> on CeO<sub>2</sub> desorbed mainly from 50 °C to 200 °C, and the desorption peak was observed at 170 °C. Relatively less amount of CO<sub>2</sub> desorption continues from 600 °C to 750 °C. Basic properties of any catalysts depend on the temperature response in the strong region of >450 °C, moderate region between 200–450 °C and weak region of <200 °C. The strong basic sites are because of the formation

of unidentate carbonate and low coordination  $O^{2-}$  ions. The moderate basic sites are due to the formation of bridged and bidentate carbonates the sites  $M^{X+}-O^{2-}$  pairs; weak basic sites are corresponds to the bicarbonate formed by the interactions between OH groups and the surface. The TPD curve indicates that  $CeO_2$  has several  $CO_2$  adsorption sites which resulted in difference between steep  $CO_2$  desorption at lower temperature and broad  $CO_2$  desorption at higher temperature.

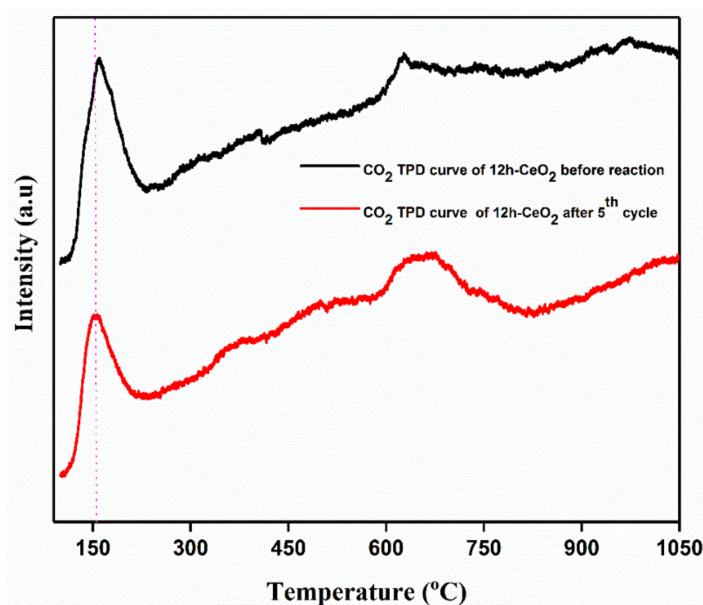


**Figure 7.**  $CO_2$  TPD curve of  $CeO_2$  testing. The curve represents amount of  $CO_2$  desorbed.

### 2.3. Dehydrating Agents and DMC Production

In addition, a set of DMC synthesis reactions have been performed using various dehydrating agent to understand and establish their role in catalyst activity. The best-optimized reaction conditions were used for these experiments i.e., 7.5 MPa pressure, 1 g catalyst and 140 °C temperatures. The results for molecular sieve 4A, 2,2-Dimethoxypropane (DMP), acetonitrile, cyclohexene oxide, styrene oxide etc. dehydrating agents are shown in Table 2. Amongst all, DMP presented best producing 1.439  $TOF\ h^{-1}$  molecular sieve 4A produces least 1.110  $TOF\ h^{-1}$  (Table 2; entries 14 and 15). Interestingly, epoxides such as cyclohexene oxide and styrene oxide exhibited excellent 1.419 and 1.433  $TOFs\ h^{-1}$ , respectively (Table 2; entries 17 and 18). These results indicate that dehydrating agents play an important role in direct DMC synthesis from  $CO_2$  and have a positive effect on DMC synthesis.

### 2.4. Reaction Mechanism Study Using FTIR Method

Based on the literature review and experimental results, DMC formation mechanism from  $CO_2$  and methanol over  $CeO_2$  has been proposed [33]. As shown in Figure 8, first methanol gets adsorbed at the  $CeO_2$  surface by chemical absorption forming methoxyl moiety through the oxygen atom.

This theoretical hypothesis is supported by FTIR analysis of  $CeO_2$  after exposing to methanol and  $CO_2$  atmosphere. The stretching frequencies of methoxyl group appeared close to 1027 and 1097  $cm^{-1}$  which correspond to three coordinate methoxyl groups and on-top methoxylgroup in Figure 9 [34].

Also, the asymmetric and symmetric  $-(CH_3)$  vibration mode of physically adsorbed methanol was observed at about 2935 and 2821  $cm^{-1}$  [35]. The monodentate methyl carbonates group form in next step by the addition insertion reaction of  $CO_2$  and methoxyl gets adsorbed on the surface of  $CeO_2$ . The FTIR stretching frequencies observed in the region of 1592, 1453 and 1338  $cm^{-1}$  were ascribed to monodentate methyl carbonate (MMC) [37,39]. Interestingly the MMC has considered as DMC formation intermediate

over  $\text{CeO}_2$  in the previous studies. In addition, the bands appeared around 1027 and  $1592\text{ cm}^{-1}$  are the characteristic of  $-(\text{CO}_3)$  from bidentate carbonate [36,37,39]. The bands at 1453 and  $1598\text{ cm}^{-1}$  are assigned for stretching frequencies of hydrogen carbonate whereas 1104, 1350 and  $1453\text{ cm}^{-1}$  correspond to  $-(\text{CO}_3)$  group of MMC [38–40]. Formation of DMC is the final step by the reaction of activated methanol and methyl carbonate group.

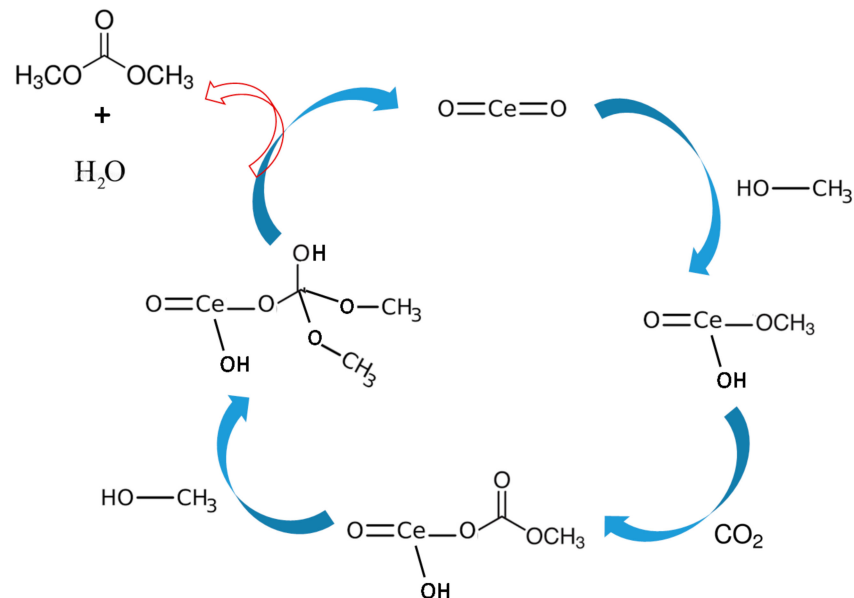


**Figure 8.** Proposed reaction mechanism based on the FTIR studies for DMC synthesis reaction over  $\text{CeO}_2$ .

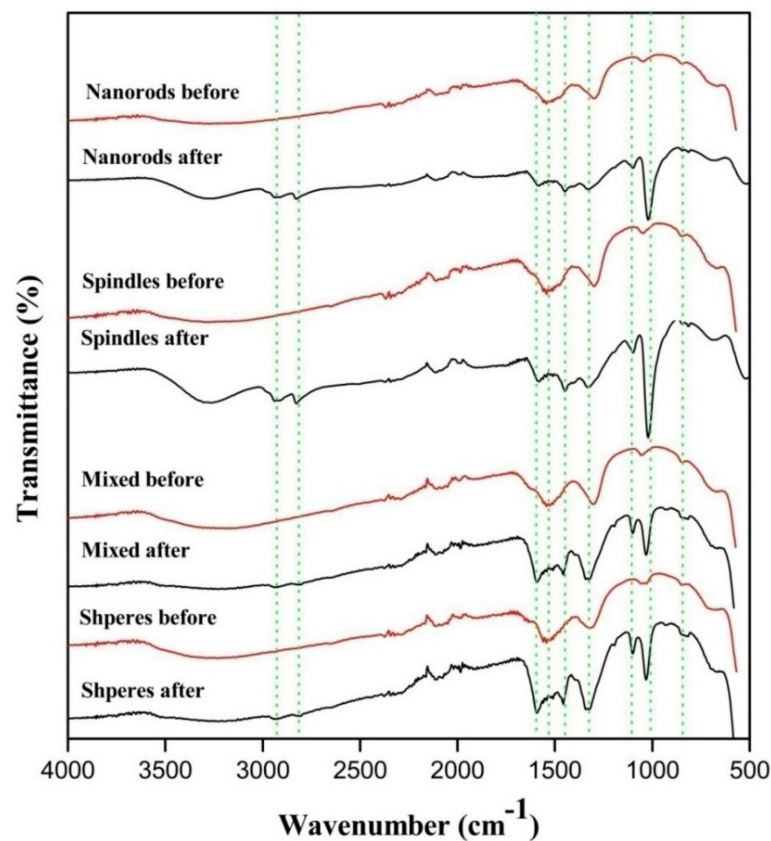


**Figure 9.** Samples before and after exposure to  $\text{CO}_2$  and methanol mixture.

### 3. Experimental Apparatus and Procedures

#### 3.1. Materials and Methods

The highly pure anhydrous DMC ( $\geq 99\%$  for gas chromatography (GC) calibration), anhydrous urea ( $\geq 98\%$ ) and cerium (III) chloride heptahydrate (99.9%) were obtained from Sigma-Aldrich, Yongin, South Korea. Potassium bromide (FTIR-grade) and anhydrous methanol (99%) were purchased from Alfa Aesar, Tewksbury, MA, USA.

A number of analytical techniques were utilized for characterization of physico-chemical properties of as-synthesized metal oxide. The morphology and microstructure of CeO<sub>2</sub> samples were investigated on a Scanning Electron Microscope (SEM, Hitachi-S-3500N, Tokyo, Japan). The samples were prepared by uniform dispersion of CeO<sub>2</sub> on carbon tape, fixed on aluminum stubs, and then sputter coated with gold-palladium for 120 s at 45 mA. An X'pertMPD diffractometer was used for XRD analysis where the diffraction angle scan was 10° (2 $\theta$ ) to 90° (2 $\theta$ ). The infrared spectra was recorded using FTIR, Varian 2000, in the range of 400–4000 cm<sup>-1</sup> having 8 cm<sup>-1</sup> resolution. Moreover, the pore diameter, pore volume and surface area of the synthesized metal oxide were determined by nitrogen adsorption-desorption using BET MODEL (BELSORP-Max [MP] from BEL Japan. Inc., Osaka, Japan). These measurements were carried out at -196 °C through the Micrometitics static volumetric analyzer. All the data regarding the porosity of the ready cerium oxides, together with the BET surface area, pore-size distribution and pore volume resulted from different models are calculated by the computer unit of BELSORP-Max [MP] analyzer. Then, Non-Local Density Functional Theory (NLDFIT) was used to check the pore size distribution using through adsorption branch and isotherms were calculated using a combination of statistical thermodynamic NLDFIT calculations. The transmission electron microscope (TEM) 160 kV (JEM-200CX), JEOL JEM-2010F (JEOL, Tokyo, Japan) high-resolution transmission electron microscope (HRTEM) and selected area electron diffraction (SAED) were employed to know the size, morphology and crystalline nature.

#### 3.2. Synthesis of Catalyst

The CeO<sub>2</sub> were synthesized using our earlier reported method [41]. In brief, 3.7 gm of cerium (III) chloride heptahydrate (0.01 mol) and 3 gm of urea (in a 1:5 molar ratio i.e., 0.05 mol) were taken in 250 mL closed borosil glass bottle (SCHOTT DURAN-00336343) having adequate water, maintaining 0.1 M concentration of metal salt. The ultrafine sonication were applied to reaction mixture in order to make it uniform and then heated in heating oven at 120 °C for 3 h. Then the reaction mixture was suction filtered with thorough distilled water and anhydrous ethanol wash to check the adsorbed byproducts on the surface of precipitate. Finally, the obtained product dried at 60 °C for 12 h and annealed at 500 °C for 3 h to obtain cerium oxide. Depending on their synthesis time (heating in oven) i.e., 8 h, 10 h, 12 h and 16 h, CeO<sub>2</sub> samples were named as sphere CeO<sub>2</sub>, mixed shape CeO<sub>2</sub>, spindle CeO<sub>2</sub>, and nanorod CeO<sub>2</sub>, respectively.

#### 3.3. Conversion of CO<sub>2</sub> and Methanol into DMC in Batch Reactor over CeO<sub>2</sub> Catalyst

In brief, 25 mL of methanol (618 mmol) and 0.5 to 2 g of CeO<sub>2</sub> catalyst (2.9 to 11.62 mmol) were added into 100 mL (SPG Co., Ltd., Incheon, South Korea) stainless steel reactor secured with PID temperature controller (Hanwoul Engineering Company, Incheon, South Korea). Then, the reactor was heated to 120 to 160 °C with stirring rate of ~900 rpm after pressurizing to the desired CO<sub>2</sub> gas. After respective reaction time, the reactor cooled down to room temperature, depressurized slowly and the catalyst was separated by simple filtration. Finally, the reaction mixture was injected in gas chromatography-mass spectroscopy (Agilent 19091J-433 GC-MS; capillary column; EI model at 70 eV) and gas chromatography (Shimadzu GC 17A; stabilwax column; flame ionization detector) for product analysis.

#### 4. Conclusions

We have successfully demonstrated the effect of CeO<sub>2</sub> morphology on product yield and catalytic activity for DMC synthesis from CO<sub>2</sub> and the study suggests that excellent DMC production can be achievable by modifying the morphology of a CeO<sub>2</sub> catalyst. We have proposed a modified cost-effective and facile precipitation method for synthesizing different morphologies of CeO<sub>2</sub> at ambient synthesis conditions. The formation mechanism of CeO<sub>2</sub> is being proposed with the help of time-dependent experiments and SEM analysis. The results showed that spindle shape of CeO<sub>2</sub> along, with higher surface area, is the most active catalyst for CO<sub>2</sub> and methanol conversion reaction. A number of experiments are carried out to determine the role of dehydrating agents. Furthermore, a DMC formation reaction mechanism over CeO<sub>2</sub> is proposed based on the stretching vibrations of CO<sub>2</sub> and methanol experiential in the FTIR spectra. The bands at 1592, 1453 and 1338 cm<sup>-1</sup> are characteristic frequencies of MMC, which indicates that MMC would be the intermediate in the DMC formation over CeO<sub>2</sub> catalyst. We believe that aside from DMC production, the spindle-shape CeO<sub>2</sub> catalyst can also work in various CO<sub>2</sub> fixation reactions, as their catalytic properties may not belimited to DMC synthesis.

**Author Contributions:** Conceptualization, A.F., and H.K.; methodology, A.H.T., H.K., S.G., C.T.; validation, C.T., S.G., H.K., and A.F.; formal analysis, A.H.T., and N.S.; investigation, A.H.T., N.S., C.T.; data curation, A.H.T.; writing—original draft preparation, A.H.T., H.K.; writing—review and editing, A.H.T., C.T., S.G.; visualization, A.F.; supervision, A.F., S.G., C.T., H.K.; project administration, A.F., C.T., S.G., H.K.; funding acquisition, C.T., and H.K. All authors have read and agreed to the published version of the manuscript.

**Funding:** This research was partly funded by MEXT Promotion of Distinctive Joint Research Center Program Grant Number JPMXP0618217662; National Research Foundation of Korea funded by the Ministry of Education (No. 2020R1A6A1A03038817) and by the Korea Institute of Energy Technology Evaluation and Planning (KETEP), funded by the Ministry of Trade, Industry & Energy (MOTIE) (No. 20194010201750) of the Republic of Korea. The APC was funded by MEXT Promotion of Distinctive Joint Research Center Program Grant Number JPMXP0618217662.

**Data Availability Statement:** Not Applicable.

**Acknowledgments:** AF, CT, NS, would like thank, MEXT Promotion of Distinctive Joint Research Center Program for financial support. SWG would like to thank UPE Phase II 263(A3), Government of India, for financials support. AT would like to thanks for funding by UGC D. S. Kothari Post-Doctoral Fellowship. H.K., would thanks for the financial support from the National Research Foundation of Korea funded by the Ministry of Education and by the Korea Institute of Energy Technology Evaluation and Planning (KETEP), funded by the Ministry of Trade, Industry & Energy (MOTIE) of the Republic of Korea.

**Conflicts of Interest:** The authors declare no conflict of interest.

#### References

1. Bian, J.; Xiao, M.; Wang, S.-J.; Lu, Y.-X.; Meng, Y.-Z. Carbon nanotubes supported Cu–Ni bimetallic catalysts and their properties for the direct synthesis of dimethyl carbonate from methanol and carbon dioxide. *Appl. Surf. Sci.* **2009**, *255*, 7188–7196. [[CrossRef](#)]
2. Leung, D.Y.C.; Caramanna, G.; Maroto-Valer, M.M. An overview of current status of carbon dioxide capture and storage technologies. *Renew. Sustain. Energy Rev.* **2014**, *39*, 426–443. [[CrossRef](#)]
3. Tamboli, H.; Chaugule, A.A.; Kim, H. Catalytic developments in the direct dimethyl carbonate synthesis from carbon dioxide and methanol. *Chem. Eng. J.* **2017**, *323*, 530–544. [[CrossRef](#)]
4. Sun, W.; Shi, R.; Wang, X.; Liu, S.; Han, X.; Zhao, C.; Li, Z.; Ren, J. Density-functional theory study of dimethyl carbonate synthesis by methanol oxidative carbonylation on single-atom Cu 1/graphene catalyst. *Appl. Surf. Sci.* **2017**, *425*, 291–300. [[CrossRef](#)]
5. Kwon, E.E.; Yi, H.; Jeon, Y.J. Boosting the value of biodiesel byproduct by the non-catalytic transesterification of dimethyl carbonate via a continuous flow system under ambient pressure. *Chemosphere* **2014**, *113*, 87–92. [[CrossRef](#)]
6. Aricò, F.; Tundo, P. Dimethyl carbonate as a modern green reagent and solvent. *Russ. Chem. Rev.* **2010**, *79*, 479–489. [[CrossRef](#)]
7. Tundo, P.; Selva, M. The chemistry of dimethyl carbonate. *Acc. Chem. Res.* **2002**, *35*, 706–716. [[CrossRef](#)]
8. Tamboli, A.H.; Bandal, H.A.; Kim, H. Solvent free synthesis of cyclic ureas and urethanes by carbonylation method in the basic dicationic ionic liquid catalysts. *Chem. Eng. J.* **2016**, *306*, 826–831. [[CrossRef](#)]

9. Zhang, G.; Li, Z.; Zheng, H.; Hao, Z.; Wang, X.; Wang, J. Influence of surface oxygenated groups on the formation of active Cu species and the catalytic activity of Cu/AC catalyst for the synthesis of dimethyl carbonate. *Appl. Surf. Sci.* **2016**, *390*, 68–77. [[CrossRef](#)]
10. Ren, Y.; Ma, Z.; Bruce, P.G. Ordered mesoporous metal oxides: Synthesis and applications. *Chem. Soc. Rev.* **2012**, *41*, 4909–4927. [[CrossRef](#)]
11. Nasreen, S.; Liu, H.; Qureshi, L.A.; Sissou, Z.; Lukic, I.; Skala, D. Cerium-manganese oxide as catalyst for transesterification of soybean oil with subcritical methanol. *Fuel Process. Technol.* **2016**, *148*, 76–84. [[CrossRef](#)]
12. Jung, K.T.; Bell, A.T. An In Situ Infrared Study of Dimethyl Carbonate Synthesis from Carbon Dioxide and Methanol over Zirconia. *J. Catal.* **2001**, *204*, 339–347. [[CrossRef](#)]
13. Kang, K.H.; Lee, C.H.; Kim, D.B.; Jang, B.; Song, I.K. NiO/CeO<sub>2</sub>-ZnO Nano-Catalysts for Direct Synthesis of Dimethyl Carbonate from Methanol and Carbon Dioxide. *J. Nanosci. Nanotechnol.* **2014**, *14*, 8693–8698. [[CrossRef](#)] [[PubMed](#)]
14. Kumar, P.; With, P.; Srivastava, V.C.; Gläser, R.; Mishra, I.M. Conversion of carbon dioxide along with methanol to dimethyl carbonate over ceria catalyst. *J. Environ. Chem. Eng.* **2015**, *3*, 2943–2947. [[CrossRef](#)]
15. Tamboli, A.H.; Gosavi, S.W.; Terashima, C.; Fujishima, A.; Pawar, A.A.; Kim, H. Synthesis of cerium and nickel doped titanium nanofibers for hydrolysis of sodium borohydride. *Chemosphere* **2018**, *202*, 669–676. [[CrossRef](#)]
16. Marin, C.M.; Li, L.; Bhalkikar, A.; Doyle, J.E.; Zeng, X.C.; Cheung, C.L. Kinetic and mechanistic investigations of the direct synthesis of dimethyl carbonate from carbon dioxide over ceria nanorod catalysts. *J. Catal.* **2016**, *340*, 295–301. [[CrossRef](#)]
17. Santos, B.A.V.; Silva, V.M.T.M.; Loureiro, J.M.; Rodrigues, A.E. Review for the Direct Synthesis of Dimethyl Carbonate. *ChemBioEng Rev.* **2014**, *1*, 214–229. [[CrossRef](#)]
18. Bansode, A.; Urakawa, A. Continuous DMC synthesis from CO<sub>2</sub> and methanol over a CeO<sub>2</sub> catalyst in a fixed bed reactor in the presence of a dehydrating agent. *ACS Catal.* **2014**, *4*, 3877–3880. [[CrossRef](#)]
19. Santos, B.A.V.; Pereira, C.S.M.; Silva, V.M.T.M.; Loureiro, J.M.; Rodrigues, A.E. Kinetic study for the direct synthesis of dimethyl carbonate from methanol and CO<sub>2</sub> over CeO<sub>2</sub> at high pressure conditions. *Appl. Catal. A Gen.* **2013**, *455*, 219–226. [[CrossRef](#)]
20. Wang, F.; Yu, H.; Tian, Z.; Xue, H.; Feng, L. Active sites contribution from nanostructured interface of palladium and cerium oxide with enhanced catalytic performance for alcohols oxidation in alkaline solution. *J. Energy Chem.* **2018**, *27*, 395–403. [[CrossRef](#)]
21. Fang, Y.; Haiying, F.; Yang, L.; Lihong, L.; Dionysios, X.; Dionysioud, D.; Yanga, L.; Xing, B. Nano-cerium oxide functionalized biochar for phosphate retention: Preparation, optimization and rice paddy application. *Chemosphere* **2017**, *185*, 816–825. [[CrossRef](#)]
22. Xu, J.; Long, K.Z.; Wu, F.; Xue, B.; Li, Y.X.; Cao, Y. Efficient synthesis of dimethyl carbonate via transesterification of ethylene carbonate over a new mesoporous ceria catalyst. *Appl. Catal. A Gen.* **2014**, *484*, 1–7. [[CrossRef](#)]
23. Wang, S.; Zhao, L.; Wang, W.; Zhao, Y.; Zhang, G.; Ma, X.; Gong, J. Morphology control of ceria nanocrystals for catalytic conversion of CO<sub>2</sub> with methanol. *Nanoscale* **2013**, *5*, 5582–5588. [[CrossRef](#)]
24. Mei, J.; Ke, Y.; Yu, Z.; Hu, X.; Qu, Z.; Yan, N. Morphology-dependent properties of Co<sub>3</sub>O<sub>4</sub>/CeO<sub>2</sub> catalysts for low temperature dibromomethane (CH<sub>2</sub>Br<sub>2</sub>) oxidation. *Chem. Eng. J.* **2017**, *320*, 124–134. [[CrossRef](#)]
25. Chen, L.; Wang, S.; Zhou, J.; Shen, Y.; Zhao, Y.; Ma, X. Dimethyl carbonate synthesis from carbon dioxide and methanol over CeO<sub>2</sub> versus over ZrO<sub>2</sub>: Comparison of mechanisms. *RSC Adv.* **2014**, *4*, 30968–30975. [[CrossRef](#)]
26. Hu, S.; Ouyang, R.; Li, W.-X. First-principles kinetics study of carbon monoxide promoted Ostwald ripening of Au particles on FeO/Pt(111). *J. Energy Chem.* **2019**, *30*, 108–113. [[CrossRef](#)]
27. Piwoński, I.; Spilarewicz-Stanek, K.; Kisielewska, A.; Kadziola, K.; Cichomski, M.; Ginter, J. Examination of Ostwald ripening in the photocatalytic growth of silver nanoparticles on titanium dioxide coatings. *Appl. Surf. Sci.* **2016**, *373*, 38–44. [[CrossRef](#)]
28. Madras, G.; McCoy, B.J. Distribution kinetics theory of Ostwald ripening. *J. Chem. Phys.* **2001**, *115*, 6699–6706. [[CrossRef](#)]
29. Gao, J.; Zhao, Y.; Yang, W.; Tian, J.; Guan, F.; Ma, Y.; Hou, J.; Kang, J.; Wang, Y. Preparation of samarium oxide nanoparticles and its catalytic activity on the esterification. *Mater. Chem. Phys.* **2003**, *77*, 65–69. [[CrossRef](#)]
30. Langford, J.I.; Wilson, A.J.C. Scherrer after sixty years: A survey and some new results in the determination of crystallite size. *J. Appl. Crystallogr.* **1978**, *11*, 102–113. [[CrossRef](#)]
31. Lee, D.K.; Park, S.I.; Lee, J.K.; Hwang, N.M. A theoretical model for digestive ripening. *Acta Mater.* **2007**, *55*, 5281–5288. [[CrossRef](#)]
32. Ghosh, A.; Chakrabarti, S.; Biswas, K.; Ghosh, U.C. Agglomerated nanoparticles of hydrous Ce(IV) + Zr(IV) mixed oxide: Preparation, characterization and physicochemical aspects on fluoride adsorption. *Appl. Surf. Sci.* **2014**, *307*, 665–676. [[CrossRef](#)]
33. Yoshikawa, K.; Sato, H.; Kaneeda, M.; Kondo, J.N. Synthesis and analysis of CO<sub>2</sub> adsorbents based on cerium oxide. *J. CO<sub>2</sub> Util.* **2014**, *8*, 34–38. [[CrossRef](#)]
34. Aresta, M.; Dibenedetto, A.; Pastore, C.; Angelini, A.; Aresta, B.; Pápai, I. Influence of Al<sub>2</sub>O<sub>3</sub> on the performance of CeO<sub>2</sub> used as catalyst in the direct carboxylation of methanol to dimethylcarbonate and the elucidation of the reaction mechanism. *J. Catal.* **2010**, *269*, 44–52. [[CrossRef](#)]
35. Chen, Y.; Tang, Q.; Ye, Z.; Li, Y.; Yang, Y.; Pua, H.; Gao, L. Monolithic Zn x Ce 1– x O 2 catalysts for catalytic synthesis of dimethyl carbonate from CO 2 and methanol. *New J. Chem.* **2020**, *44*, 12522–12530. [[CrossRef](#)]
36. Vayssilov, G.N.; Mihaylov, M.; Petkov, P.S.; Hadjiivanov, K.I.; Neyman, K.M. Reassignment of the vibrational spectra of carbonates, formates, and related surface species on ceria: A combined density functional and infrared spectroscopy investigation. *J. Phys. Chem. C* **2011**, *115*, 23435–23454. [[CrossRef](#)]
37. Monteiro, R.S.; Noronha, F.B.; Dieguez, L.C.; Schmal, M. Characterization of PdCeO<sub>2</sub> interaction on alumina support and hydrogenation of 1, 3-butadiene. *Appl. Catal. A Gen.* **1995**, *131*, 89–106. [[CrossRef](#)]

38. Marciniaka, A.A.; Henrique, F.J.F.S.; Lima, A.F.F.; Alves, O.; Moreira, C.R.; Appele, L.G.; Mota, C.J.A. What are the preferred CeO<sub>2</sub> exposed planes for the synthesis of dimethyl carbonate? Answers from theory and experiments. *Mol. Catal.* **2020**, *493*, 111053. [[CrossRef](#)]
39. Pozdnyakova, O.; Teschner, D.; Wootsch, A.; Kröhnert, J.; Steinhauer, B.; Sauer, H.; Toth, L.; Jentoft, F.C.; Knop-Gericke, A.; Paál, Z.; et al. Preferential CO oxidation in hydrogen (PROX) on ceria-supported catalysts, part II: Oxidation states and surface species on Pd/CeO<sub>2</sub> under reaction conditions, suggested reaction mechanism. *J. Catal.* **2006**, *237*, 17–28. [[CrossRef](#)]
40. Binet, C.; Daturi, M.; Lavalley, J.-C. {IR} study of polycrystalline ceria properties in oxidised and reduced states. *Catal. Today* **1999**, *50*, 207–225. [[CrossRef](#)]
41. Durano, M.M.; Tamboli, A.H.; Kim, H. Cobalt oxide synthesized using urea precipitation method as catalyst for the hydrolysis of sodium borohydride, Colloids Surfaces a Physicochem. *Eng. Asp.* **2017**, *520*, 355–360. [[CrossRef](#)]